Published in final edited form as:
Acta Neuropathol. 2011 September ; 122(3): 331–341. doi:10.1007/s00401-011-0848-5.

The spinal muscular atrophy mouse model, SMAΔ7, displays altered axonal transport without global neurofilament alterations

Jeffrey M. Dale,
Division of Biological Sciences, University of Missouri-Columbia, Columbia, MO 65211, USA. 345 C.S. Bond Life Sciences Center, University of Missouri-Columbia, 1201 Rollins Rd, Columbia, MO 65211, USA

Hailian Shen,
345 C.S. Bond Life Sciences Center, University of Missouri-Columbia, 1201 Rollins Rd, Columbia, MO 65211, USA

Devin M. Barry,
Division of Biological Sciences, University of Missouri-Columbia, Columbia, MO 65211, USA. 345 C.S. Bond Life Sciences Center, University of Missouri-Columbia, 1201 Rollins Rd, Columbia, MO 65211, USA

Virginia B. Garcia,
345 C.S. Bond Life Sciences Center, University of Missouri-Columbia, 1201 Rollins Rd, Columbia, MO 65211, USA

Ferrill F. Rose Jr,
Veterinary Pathology/Molecular Microbiology and Immunology, University of Missouri-Columbia, Columbia, MO 65211, USA. 403 C.S. Bond Life Sciences Center, University of Missouri-Columbia, 1201 Rollins Rd, Columbia, MO 65211, USA

Christian L. Lorson, and
Veterinary Pathology/Molecular Microbiology and Immunology, University of Missouri-Columbia, Columbia, MO 65211, USA. 471G C.S. Bond Life Sciences Center, University of Missouri-Columbia, 1201 Rollins Rd, Columbia, MO 65211, USA

Michael L. Garcia
Division of Biological Sciences, University of Missouri-Columbia, Columbia, MO 65211, USA. 340C C.S. Bond Life Sciences Center, University of Missouri-Columbia, 1201 Rollins Rd, Columbia, MO 65211, USA

Michael L. Garcia: GarciaML@missouri.edu

Abstract

Spinal muscular atrophy (SMA) is a neurodegenerative disease resulting from decreased levels of survival motor neuron 1 (SMN1) protein. Reduced SMN1 levels are linked to pathology at neuromuscular junctions (NMJs), which includes decreased vesicle density and organization, decreased quantal release, increased endplate potential duration, and neurofilament (NF) accumulations. This work presents a first study towards defining molecular alterations that may lead to the development of NMJ pathology in SMA. Fast, anterograde transport of synaptic vesicle

Correspondence to: Michael L. Garcia, GarciaML@missouri.edu.

Present Address: H. Shen, Department of Neurology, LRB 670Z, University of Massachusetts Medical School, Worcester, MA 01605, USA

Conflict of interest None.

2 (SV2-c) and synaptotagmin (Syt1) proteins was reduced 2 days prior to the observed decrease in synaptic vesicle density. Moreover, reduced accumulation of SV2-c or Syt1 was not due to reduced protein expression or reduced kinesin activity. Dynein levels were reduced at times that are consistent with NF accumulations at NMJs. Furthermore, NF distribution, from cell body to sciatic nerve, appeared normal in SMAΔ7 mice. Taken together, these results suggest that reduced axonal transport may provide a mechanistic explanation for reduced synaptic vesicle density and concomitant synaptic transmission defects, while providing evidence that suggests NF accumulations result from local NMJ alterations to NFs.

Keywords

Axonal transport; Neurofilaments; NMJ; SMA; Synaptic release

Introduction

Spinal muscular atrophy (SMA) is an autosomal recessive disorder that is the leading genetic cause of infantile death [18]. SMA is a severe neuromuscular disease characterized by paralysis of skeletal muscle [14, 17]. SMA is caused by a deficiency in survival motor neuron (SMN) protein levels [15, 16], which is a ubiquitously expressed protein that has a well described role in RNA metabolism [4, 19, 27]. It is not currently known why low levels of this ubiquitously expressed protein selectively affect α-motor neurons.

In a well-established SMA model, SMAΔ7 [14], motor neurons from different spinal segments are differently affected by SMN deficiencies. Motor neuron loss was observed in the fourth cervical ventral root [11], while motor neuron number in the fourth [11] and fifth [22] lumbar ventral roots remains unchanged in the SMAΔ7 model. Despite these differences, there are common alterations within axons of SMA mice. NF accumulations are observed as early as P5 and progress to ~90% occupancy of all observed NMJs by P14 [11]. Starting at P7, SMAΔ7 mice develop a progressive attenuation of evoked responses where evoked endplate potential (EPP) traces show increased rising and falling phase durations in the transversus abdominis (TVA) muscle [23]. At P10, attenuated EPP response can be seen in the tibialis anterior (TA) muscle [12]. By P13, SMAΔ7 mice have a significant reduction in total synaptic vesicles and docked synaptic vesicles at TA NMJs [12]. Consistently, by P14, SMAΔ7 quantal release is reduced by ~50% relative to wild-type mice in both the TA muscle [12] and TVA muscle [23] suggesting a defect in vesicle positioning.

Although NMJ structural and functional abnormalities have been clearly defined in muscles innervated by thoracic motor neurons (TVA) and lumbar motor neurons (TA), the mechanisms through which these alterations occur have remained unexplored. Branches of the sciatic nerve show both NMJ NF accumulations [3, 11, 12] and decreased synaptic vesicles [12]. Therefore, we focused our study on the sciatic nerve. Moreover, the mouse sciatic nerve consists of the fourth, fifth and sixth lumbar spinal segments [20] making it a large easily accessible nerve contrary to the nerves that innervate proximal muscles. In this study, we have performed the first in vivo analysis of NF organization and fast axonal transport along the sciatic nerve in SMAΔ7 mice. Our results suggest that NF accumulations at the NMJ are due to local alterations to NF dynamics. Furthermore, our results indicate that alterations in fast, anterograde cargo transport precede the observed decrease in synaptic vesicle density [12] and reduced quantal release [23] in the TA muscle suggesting that axonal transport defects may contribute to SMA pathogenesis.

Materials and methods

Animals and genotyping

All procedures were in compliance with the University of Missouri Animal Care and Use Committee and with all local and federal laws governing the humane treatment of animals. Mice were housed in microisolator cages on a 12-h light/dark cycle and were given food and water ad libitum. SMAΔ7 mice on a FVB/N background were purchased from Jackson Laboratories. SMAΔ7 mice were generated by crossing mSMN±; hSMNΔ7+/+; hSMN2+/+ mice.

For quantitative real-time PCR, RNA was isolated from brain tissue using TriReagent protocol and treated with RQ1 DNase to eliminate genomic and transgenic DNA. Equal amounts of total RNA were used to make the cDNA. Omitting reverse transcriptase was used as a negative control. Quantitative real-time PCR was performed using TaqMan and primers described previously [25].

Mice were genotyped at the SMN locus using the following primers: wild type forward 5′-TCTGTGTTCGTGCGTGGTGACTTT-3′, wild-type reverse 5′-CCCACCACCTAAGAAAGCCTCAAT-3′, LacZ forward 5′-CC AACTTAATCGCCTTGCAGCACA-3′, LacZ Reverse 5′-AAGCGAGTGGCAACATGGAAATCG-3′. Primers result in wild type and targeted bands of 372 and 626 bp, respectively.

PCR protocols were set-up using a 0.8 μM final concentration of each primer and had the following cycling parameters: initial denaturing of 2 min at 94°C; 36 cycles of 15 s at 94°C and 1 min at 68°C; followed by a final elongation of 10 min at 68°C.

Immunofluorescence

Mice were euthanized with isoflurane and transcardially perfused with 4% paraformaldehyde/PBS. Tissues were removed by dissection and post-fixed for 1–2 h at 4°C, followed by cryoprotection in 20% sucrose/PBS overnight. Lumbar spinal cords were sectioned into 20 μm sections using a Cryostat Leica CM1900 (Northern Instrument Company). Sciatic nerves were sectioned into proximal and distal sections using a fine scissor (Fine Science Tools). Tissues were blocked for an hour at room temperature (RT) with 1% BSA (Sigma), 0.2% fat-free milk (Vons), 5% normal goat serum (Vector labs), in 1× TBS-T (0.1% Triton X-100, pH 6.8). Tissues were incubated overnight in primary antibody at RT. Primary antibodies: SMI-31 (Covance), SMI-32 (Covance), and Kif5c (Goldstein lab) at 1:1,000. Tissues were washed three times in TBS-T for 5 min, incubated for 1 h with Alexa Fluor 594 goat anti-mouse secondary antibody (Invitrogen) 1:5,000, and washed three times in TBS-T at RT. Tissues were imaged using a slit aperture Olympus BX61 w/DSU confocal microscope.

Electron micrograph and NF spacing counts

For EM analysis, mice were perfused intracardially with 4% paraformaldehyde and 2.5% glutaraldehyde in 0.1 M Sorenson’s phosphate buffer, pH 7.2, and postfixed overnight in the same buffer. Fifth lumbar nerve roots were dissected, treated with 2% osmium tetroxide, washed, dehydrated, and embedded in Epon–Araldite resin. Thin sections (60–90 nm) were cut from prepared fifth lumbar root resin blocks with a Leica Ultracut UCT ultramicrotome, collected on grids, stained with 1% aqueous uranyl acetate for 15 min followed by lead citrate for 2 min. Images of selected axons were collected at 80 kV with a JEOL-1400 transmission electron microscope at magnifications of 5,000, 10,000, or 20,000. Positions of individual neurofilaments were marked with an electronic pointer using IMOD software

(University of Colorado, Boulder), and nearest neighbor distances were calculated using software written by Stephen Lamont (NCMIR; University of California, San Diego). Statistical analysis was run using SigmaPlot for nearest neighbor distance analysis and InStat for microtubule and NF densities. NF densities were analyzed for statistical significance by Student's *t* test, and microtubule densities were analyzed by Mann–Whitney test.

Sciatic nerve ligations

The sciatic nerves of anesthetized mice were ligated with 6–0 surgical thread as previously described [6]. The tie was placed between the sciatic notch and the knee joint. After 6 h, both the ligated nerve and control (unligated) nerves were extracted from each animal and stored at −80°C.

Sciatic nerve preparation and western blot analysis

Mice were euthanized by isoflurane overdose. Total protein extracts were obtained by homogenization in 50 mM Tris(pH 7.5), 150 mM NaCl, 5 mM EDTA, 1 mM protease inhibitors (Roche): Leupeptin, Aprotinin, Chymostatin and PMSF (20% w/v) and lysed with 50 mM Tris (pH 7.5), 150 mM NaCl, 1% NP-40, 1% deoxycholate, 2% SDS and 1 mM protease inhibitors. The samples were then sonicated at a 30% duty cycle and output control at 1 for 15 strokes followed by a 10 min boil at 100°C and centrifugation for 5 min at RT. Protein concentration was determined by Bradford assay (Bio-Rad inc.).

Cytoskeletal proteins (5 μg) were separated on a 7.5 SDS-page gel then blotted on a nitrocellulose membrane. Antibodies for CPCA NF-H (EnCor Biotech Inc.) 1:25,000, RM044 (Abcam) 1:2,000, DA2 (EnCor Biotech. Inc.) 1:4,000, and Tuj1 (Covance) 1:8,000 were used. The NF subunit proteins were identified with IRDye 700DX conjugated secondary antibodies (Rockland) and imaged with an infrared Odyssey 3000 scanner (Li-Cor). Tubulin was identified with a goat anti-rabbit IgG HRP conjugated secondary antibody (Thermo Scientific) and imaged with SuperSignal West ECL detection kit (Thermo Scientific).

Transport motors and cargo proteins (20 μg), Dynein, Kif5c, SV2-c, and Syt1, were separated on a 7.5% SDS-page gel. The Kif5c antibody was a generous gift from Dr. Lawrence S. B. Goldstein. Antibodies for Dynein IC1/2, cytosolic (E9) (Santa Cruz) 1:1,000, Kif5c 1:1,000, SV2-c (international hybridoma bank) 1:1,000 and mAb48 (international hybridoma bank) 1:1,000 were used. Kif5c was identified with goat anti-rabbit IgG HRP conjugated secondary antibodies (Thermo Scientific) 1:2,000. Dynein, Syt1, and SV2-c were indentified with goat anti-mouse IgG HRP conjugated antibodies (Thermo Scientific) 1:2,000. Imaging was achieved using a SuperSignal West ECL detection kit (Thermo Scientific).

Relative optical densities (RODs) were calculated as follows: [(transport protein mean intensity − background mean intensity)(number of pixels)]/[(control protein mean intensity − background mean intensity)(number of pixels)]. For example [(135.67 − 65.52)(1,708)/(102.05 − 7.17) (264)] is the calculation for the wild-type LP SV2-c ROD for P7 mice. Absolute intensities were obtained using Adobe Photoshop. Statistical analysis was run using SigmaPlot. Statistical significance on RODs was determined by a Student's *t* test. Each *N* contains sciatic nerves pooled from four mice.

Results

NF content and organization is unaffected along the length of motor axons

Recent evidence has suggested that NF accumulations occur near NMJs in animal models of SMA [3, 11, 12, 17]. It is unclear if NF accumulations result from the alterations to local NF dynamics or if they are indicative of alterations in NF dynamics throughout the length of motor neurons. Therefore, we analyzed NF content and organization along the length of sciatic nerve in SMAΔ7 mice. We chose to perform our analysis within the sciatic nerve, as this is one of the nerves in which both NMJ NF accumulations [3, 11, 12] and decreased synaptic vesicle densities [12] have been reported. Moreover, our analysis was not confounded by axonal loss seen in other spinal regions [11, 12].

We examined motor neuron morphology and ectopic NF accumulation at P11 and P16 in lumbar (Fig. 1a) motor neurons. Our SMAΔ7 model dropped 10% of its body mass at P11, and P16 was defined as disease end stage [14]. Motor neuron morphology was analyzed with an antibody that recognizes neurofilament heavy (NF-H) and medium (NF-M) subunits in a phospho-independent manner (SMI-32). At each time point, morphology was similar in SMAΔ7 and wild type lumbar (Fig. 1a) motor neurons. Although subtle DAPI/SMI31 overlapping staining was observed in the SMI31 (phosphorylated NFs) panels in both wild type and SMAΔ7 mice, ectopic accumulation of phosphorylated NFs was not associated with SMA cellular pathology indicated by the lack of gross cytoplasmic staining (Fig. 1a).

The absence of ectopic accumulations was not due to decreased NF expression in SMAΔ7 mice. In two independent Alzheimer's disease (AD) transgenic models, disease pathology included increases in NF-H and NF-M phosphorylated eptitopes in the lumbar spinal cord [13]. In our study, total levels of phosphorylated (SMI-31) and dephosphorylated (SMI-32) NF-H and NF-M were unaffected in spinal tissue of SMAΔ7 ($N = 3$) and wild type ($N = 3$) mice (Fig. 1b–d). NF-L was used as a loading control.

Within the axon, NFs are regularly spaced, and are required for establishing the diameter of myelinated motor axons [5]. Therefore, we analyzed NF organization in proximal motor axons of P12 SMAΔ7 mice. Qualitatively, NF networks appeared similar in low as well as high magnification (region identified by black box in lower magnification) images of SMAΔ7 and wild type motor axons (Fig. 2a). Quantification of the spacing between adjacent NFs (nearest neighbor distance) revealed that overall organization of the NF network was similar in SMAΔ7 mice (Fig. 2b). Both NF populations had a peak distance of 30–40 nm. However, SMAΔ7 ($N = 7$) axons had more NFs within the 15–25 nm range whereas wild type ($N = 9$) axons had slightly more NFs within the 45–55 nm range. The differences in the distributions of nearest neighbor distances were statistically significant ($P < 0.001$). NF density was unaffected in SMAΔ7 ($N = 7$) relative to wild type mice ($N = 9$, Fig. 2c). Recent studies suggest that NF amino terminal head domains bind tubulin inhibiting microtubule assembly [1]. Therefore, increased microtubule density would suggest a reduction in NFs. We measured the density of microtubules in SMAΔ7 ($N = 7$) and wild-type mice ($N = 9$, Fig. 2d). Although the density of microtubules was reduced in SMAΔ7 mice, these differences did not reach statistical significance (Fig. 2d).

Sciatic nerve ligations were used to block the transport of cargos associated with anterograde and retrograde motors. In P7 animals, we observed intense, localized kinesin (Kif5c) signals on the proximal and distal side of the ligation. Because kinesin is the anterograde transport motor [6] and is recycled to the cell body by retrograde transport motors [6], we expected accumulations on both sides of the ligation. We did not observe accumulation of Kif5c in an unligated control demonstrating normal kinesin motor

distribution (Fig. 3). Proximal and distal segments in unligated nerves approximate the location of the ligature site (Fig. 3).

NF content was analyzed in proximal and distal segments of the sciatic nerve in P7 (Fig. 4a) and P11 (Fig. 4c) SMAΔ7 ($N = 3$) and wild type ($N = 3$) littermates. Sciatic nerve lysates were immunoblotted with antibodies recognizing mouse NF-H (CPCA NF-H), NF-M (RMO44), NF-L (DA2) and a neuron specific isoform of tubulin, βIII-tubulin (TUJ1). There was no difference in NF or microtubule content in sciatic nerves at both time points. Relative optical density (ROD) measurements were used to quantify accumulation levels at P7 (Fig. 4b) and P11 (Fig. 4d). Taken together, these analyses suggested that NF accumulations at the NMJ might have resulted from a local disruption to NF dynamics rather than alterations along the length of motor axons, such as alterations in NF transport.

Defects in fast, anterograde transport cargos occur prior to the observed decrease in synaptic vesicle density

Our analysis of NF organization suggested that NF delivery was not affected in SMAΔ7 mice. We next analyzed cargos associated with fast axonal transport to determine if disrupted fast transport contributes to disease pathogenesis in SMAΔ7 mice. For anterograde transport, we analyzed the accumulation of synaptic vesicle protein 2 (SV2-c), synaptotagmin (Syt1), and Kif5c in ligated sciatic nerves. Dynein accumulation was utilized to monitor retrograde transport. Sciatic nerves were ligated for 6 h in P7 (Fig. 5) and P11 (Fig. 6) wild type and SMAΔ7 littermates. A 2-h ligation time was sufficient to clearly observe accumulation of synaptotagmin and SV2 [28]. At P7, the accumulation of SV2-c ($N = 3$) and Syt1 ($N = 5$) appeared similar in SMAΔ7 and wild-type mice suggesting unaltered protein transport (Fig. 5a). Accumulation of Kif5c ($N = 4$), and dynein ($N = 3$, Fig. 5c) appeared similar supporting the conclusion that fast axonal transport is unaltered in P7 SMAΔ7 mice. ROD measurements were used to quantify the accumulation of transport cargos (Fig. 5b) and motors (Fig. 5d) compared to a NF-H control.

However, in P11 SMAΔ7 mice, accumulation of SV2-c ($N = 3$) was reduced on the proximal side of the ligation ($P < 0.001$). Since SV2-c is an anterogradely transported protein, decreased accumulation on the cell body side (proximal) suggests that SV2-c is not being transported as efficiently along the sciatic nerve. SV2-c levels were also decreased in distal sciatic nerve sections in unligated nerves suggesting a lack of SV2-c labeled vesicles at the distal axon (Fig. 6a). However, the differences did not reach statistical significance (Fig. 6b). Syt1 ($N = 4$) levels also appeared reduced distally in both ligated ($P < 0.01$) and unligated ($P < 0.01$) nerves relative to control mice suggesting that SMAΔ7 mice have decreased Syt1 labeled vesicles on the NMJ side (distal) of the sciatic nerve (Fig. 6a). ROD measurements confirmed that levels of both proteins were reduced relative to a NF-H control (Fig. 6b). Interestingly, Kif5c ($N = 3$) accumulation appeared unaltered, whereas dynein ($N = 4$) accumulation appeared reduced on the proximal ($P < 0.05$) and distal ($P < 0.05$) side of the ligature site indicating decreased steady state levels and retrograde transport in ligated nerves (Fig. 6c). Dynein levels appeared reduced in proximal and distal sections of unligated nerves. However, the decreases did not reach statistical significance. ROD measurements again confirmed that Kif5c accumulation was unaffected and dynein accumulation was reduced compared with a NF-H control (Fig. 6d).

Increased accumulation of synaptic vesicle proteins in spinal cords of SMAΔ7 mice

Kif5c accumulated to wild-type levels at both analyzed time points suggesting that altered transport of synaptic vesicle proteins is not the result of altered kinesin mobility. However, decreased accumulation of synaptic vesicle proteins may have been due to altered expression of these proteins. To determine if SMAΔ7 mice had decreased levels of synaptic

vesicle proteins, SV2-c and Syt1, we analyzed spinal cords from P7 ($N = 3$, Fig. 7a) and P11 ($N = 5$, Fig. 7c) wild type and SMAΔ7 littermates. SV2-c levels appeared to be increased in SMAΔ7 spinal cord extracts at both P7 ($P < 0.05$) and P11 ($P < 0.05$) in 10 and 20 μg assays, whereas Syt1 levels appeared unaltered at both time points (Fig. 7a, c). ROD measurements confirmed these observations at P7 (Fig. 7b) and P11 (Fig. 7d) compared with a NF-H control. Taken together, these data suggest that decreased transport of synaptic vesicle proteins is not due to decreased expression of these proteins.

Discussion

As with many neurodegenerative diseases, SMA is caused by the severe reduction of a ubiquitously expressed protein. It is unclear how low levels of SMN selectively affect α-motor neurons. In SMA animal models, several different nerves have been analyzed. While there are differences in survival of motor neurons from different spinal segments, common pathological hallmarks have been identified in NMJs of SMAΔ7 nerves. Progressive accumulations of NFs [11] and altered electrophysiological properties [12, 23] due to reduced synaptic vesicles are common in both the transversus abdominis (TVA) and tibialis anterior (TA) muscles. Our analysis was performed on the sciatic nerve as it offered several advantages over thoracic nerves. The sciatic nerve consists of the fourth, fifth and sixth lumbar spinal nerves [20] making it a large nerve that is easily accessible prior to branching. Motor neuron loss has not been observed in fourth [11] and fifth [21] lumbar motor roots. Therefore, decreasing axon number did not confound interpretation of our results. In addition, pathological alterations in the sciatic nerve NMJs occur later in disease progression than proximal nerves [11]. At P2, none of the NMJs associated with the gastrocnemius (innervated by a branch of the sciatic nerve) are positive for NF accumulations compared to ~25% of NMJs innervating proximal muscles [11]. Therefore, no overt pathology has occurred at a time when mice have grown to a sufficient size making surgical ligation technically more feasible. Furthermore, we were able to track disease progression more effectively due to the late onset of morphological abnormalities.

NF accumulations might act as a physical barrier in the distal axon contributing to SMA pathogenesis. Therefore, we were interested in determining if NF accumulations at NMJs were due to local alterations or indicative of changes along the length of the sciatic nerve. Increased NF post-translational modifications preceded neurodegeneration in mouse models of AD [7, 13] and NF phosphorylation has been shown to play a critical role in NF organization and trafficking [8, 29]. Therefore, we analyzed NF phosphorylation at the motor neuron cell bodies. We found no differences in total NF content or phosphorylated NF content in our SMAΔ7 mice. Analysis of the motor root demonstrated that the NF network in the proximal axon is unaffected in our SMAΔ7 mice. Our data demonstrate that NF levels in axonal cell body, motor root, and sciatic axon are unchanged. Our findings agree with previous studies demonstrating unaltered NF levels in spinal cord and sciatic nerves derived from mice completely lacking neuronal SMN expression [3]. Therefore, NF accumulations at the NMJ may have resulted from local alterations in NF dynamics.

We also analyzed fast axonal transport cargos in SMAΔ7 mice. Our analysis of fast axonal transport cargos suggested that synaptic vesicle proteins were not transported into the axon as efficiently in P11 SMAΔ7 mice. Decreased transport was not due to decreased levels of synaptic vesicle proteins. In fact, we observed increased levels of SV2-c in SMAΔ7 spinal cords. Moreover, decreased transport was not due to impaired kinesin function. The kinesin heavy chain, Kif5c, is predominantly utilized in kinesin oligomer formation in motor neurons [10]. Since Kif5c accumulation was not altered in SMAΔ7, reduced transport of synaptic vesicle proteins was not due to generalized defects in anterograde transport of the selectively affected motor neurons. Instead, altered transport may be due to altered SMN

dependent processing of mRNA transcripts for synaptic vesicle proteins or kinesin subunits associated with cargo binding. For example, the TPR domain of kinesin light chain interacts with APP [9] and the tail domain of fungal conventional kinesin binds transport cargos [24]. Reduced association of transport cargos with molecular motors could account for reduced efficiency of transport and excess SV2-c localization in SMAΔ7 spinal cords. Interestingly, unlike Kif5c, dynein alterations were observed in SMAΔ7 mice. Reduced accumulation of dynein may have resulted from altered retrograde transport due to NF accumulations. NF accumulations at the NMJ are distinguishable at P5, occupy ~50% of all observed NMJs by P8, and progress to ~90% occupancy of all observed NMJs by P14 in the gastrocnemius muscle, which is innervated by a branch of the sciatic nerve [11].

Alterations in anterograde transport of synaptic vesicle proteins may provide mechanistic insight for several pathological alterations observed in SMAΔ7 mice. The earliest observed morphological abnormality in a muscle innervated by a branch of the sciatic nerve is NF accumulations at P5 [11]. Starting at P7, SMAΔ7 mice develop a progressive attenuation of evoked responses where evoked endplate potential (EPP) traces show increased rising and falling phase durations in the TVA muscle [23]. At P10, the progressive EPP attenuation can also be seen in the TA muscle [12]. At P12, more than 50% of SMAΔ7 mice failed to right themselves from a prone position [21]. However, the number of motor neurons and the distribution of motor neuron axonal diameters were unaltered in the fourth [11] and fifth [21] lumbar motor roots of SMAΔ7 mice. By P13, SMAΔ7 mice have a significant reduction in total synaptic vesicles and docked synaptic vesicles at TA NMJs [12]. Consistently, by P14, SMAΔ7 quantal release is reduced by ~50% relative to wild type mice in both the TA [12] and TVA muscles [23] suggesting a defect in vesicle positioning. Our observed reductions in transport of SV2-c and Syt1 preceded decreases in synaptic vesicle densities by 2 days [12] and decreases in quantal release by 3 days [12, 23]. SV2-c is an accepted marker for synaptic vesicles [2]. Therefore, reduced synaptic vesicle densities at SMAΔ7 NMJs may have resulted from reduced synaptic vesicle transport. Moreover, Syt1 has been shown to have an essential role in synaptic vesicle positioning for synchronous vesicle release [26]. Decreased Syt1 transport may lead to reduced association of existing synaptic vesicles within synaptic active zones [12]. Furthermore, a reduction in the readily releasable pool of vesicles may account for the progressive elongation of evoked EPP traces that are clearly discernable by P14 [23].

Our analysis represents the first in vivo analysis of proximal to distal NF content and fast axonal transport in SMAΔ7 mice. Taken together, our data suggested that transport of synaptic vesicle proteins was impaired independent of global NF perturbations. More importantly, our studies demonstrated a decline in fast axonal transport consistent with the progressive loss of evoked EPP [23] and prior to observed reductions synaptic vesicle density at the NMJ [12].

Acknowledgments

This work was supported by Grants from National Institutes of Health [Grant number NS060073] and Charcot-Marie-Tooth Association [Grant number C00014627] and University of Missouri Research Board to MLG and by Grants from National Institutes of Health [Grant numbers R01HD054413 and R01NS041584] to CLL. Salary support for MLG was provided by the University of Missouri-Columbia and the C.S. Bond Life Sciences Center. JMD was supported by an ARRA supplement to T32 GM008396. HS was supported by Charcot-Marie-Tooth Association [Grant number C00014627] to MLG. DMB was supported by both the C.S. Bond Life Sciences Fellowship Program and the Graduate Assistance in Areas of National Need Fellowship Program. We thank the following: Electron Microscopy Core Facility at the University of Missouri for assistance with tissue preparation and with electron microscopic analysis, Mr. Steve Lamont for writing the scripts used in automated determination of numbers of NFs in assigned groups for nearest neighbor distance profiles, and Dr. Emmanual Liscum and Dr. David Schulz for comments and insights that improved this manuscript.

References

1. Bocquet A, Berges R, Frank R, et al. Neurofilaments bind tubulin and modulate its polymerization. J Neurosci. 2009; 29:11043–11054. [PubMed: 19726663]
2. Buckley K, Kelly RB. Identification of a transmembrane glycoprotein specific for secretory vesicles of neural and endocrine cells. J Cell Biol. 1985; 100:1284–1294. [PubMed: 2579958]
3. Cifuentes-Diaz C, Nicole S, Velasco ME, et al. Neurofilament accumulation at the motor endplate and lack of axonal sprouting in a spinal muscular atrophy mouse model. Hum Mol Genet. 2002; 11:1439–1447. [PubMed: 12023986]
4. Gabanella F, Butchbach ME, Saieva L, et al. Ribonucleoprotein assembly defects correlate with spinal muscular atrophy severity and preferentially affect a subset of spliceosomal snRNPs. PLoS One. 2007; 2:e921. [PubMed: 17895963]
5. Garcia ML, Rao MV, Fujimoto J, et al. Phosphorylation of highly conserved neurofilament medium KSP repeats is not required for myelin-dependent radial axonal growth. J Neurosci. 2009; 29:1277–1284. [PubMed: 19193875]
6. Hanlon DW, Yang Z, Goldstein LS. Characterization of KIFC2, a neuronal kinesin superfamily member in mouse. Neuron. 1997; 18:439–451. [PubMed: 9115737]
7. Higuchi M, Lee VM, Trojanowski JQ. Tau and axonopathy in neurodegenerative disorders. Neuromolecular Med. 2002; 2:131–150. [PubMed: 12428808]
8. Jung C, Lee S, Ortiz D, et al. The high and middle molecular weight neurofilament subunits regulate the association of neurofilaments with kinesin: inhibition by phosphorylation of the high molecular weight subunit. Brain Res Mol Brain Res. 2005; 141:151–155. [PubMed: 16246456]
9. Kamal A, Stokin GB, Yang Z, Xia CH, Goldstein LS. Axonal transport of amyloid precursor protein is mediated by direct binding to the kinesin light chain subunit of kinesin-I. Neuron. 2000; 28:449–459. [PubMed: 11144355]
10. Kanai Y, Okada Y, Tanaka Y, et al. KIF5C, a novel neuronal kinesin enriched in motor neurons. J Neurosci. 2000; 20:6374–6384. [PubMed: 10964943]
11. Kariya S, Park GH, Maeno-Hikichi Y, et al. Reduced SMN protein impairs maturation of the neuromuscular junctions in mouse models of spinal muscular atrophy. Hum Mol Genet. 2008; 17:2552–2569. [PubMed: 18492800]
12. Kong L, Wang X, Choe DW, et al. Impaired synaptic vesicle release and immaturity of neuromuscular junctions in spinal muscular atrophy mice. J Neurosci. 2009; 29:842–851. [PubMed: 19158308]
13. Lazarov O, Morfini GA, Pigino G, et al. Impairments in fast axonal transport and motor neuron deficits in transgenic mice expressing familial Alzheimer's disease-linked mutant presenilin 1. J Neurosci. 2007; 27:7011–7020. [PubMed: 17596450]
14. Le TT, Pham LT, Butchbach ME, et al. SMNDelta7, the major product of the centromeric survival motor neuron (SMN2) gene, extends survival in mice with spinal muscular atrophy and associates with full-length SMN. Hum Mol Genet. 2005; 14:845–857. [PubMed: 15703193]
15. Monani UR, Coovert DD, Burghes AH. Animal models of spinal muscular atrophy. Hum Mol Genet. 2000; 9:2451–2457. [PubMed: 11005801]
16. Monani UR, Sendtner M, Coovert DD, et al. The human centromeric survival motor neuron gene (SMN2) rescues embryonic lethality in Smn(−/−) mice and results in a mouse with spinal muscular atrophy. Hum Mol Genet. 2000; 9:333–339. [PubMed: 10655541]
17. Murray LM, Comley LH, Thomson D, et al. Selective vulnerability of motor neurons and dissociation of pre- and post-synaptic pathology at the neuromuscular junction in mouse models of spinal muscular atrophy. Hum Mol Genet. 2008; 17:949–962. [PubMed: 18065780]
18. Pearn J. Incidence, prevalence, and gene frequency studies of chronic childhood spinal muscular atrophy. J Med Genet. 1978; 15:409–413. [PubMed: 745211]
19. Pellizzoni L, Kataoka N, Charroux B, Dreyfuss G. A novel function for SMN, the spinal muscular atrophy disease gene product, in pre-mRNA splicing. Cell. 1998; 95:615–624. [PubMed: 9845364]
20. Rigaud M, Gemes G, Barabas ME, et al. Species and strain differences in rodent sciatic nerve anatomy: implications for studies of neuropathic pain. Pain. 2008; 136:188–201. [PubMed: 18316160]

21. Rose FF Jr, Mattis VB, Rindt H, Lorson CL. Delivery of recombinant follistatin lessens disease severity in a mouse model of spinal muscular atrophy. Hum Mol Genet. 2009; 18:997–1005. [PubMed: 19074460]
22. Rose FF Jr, Meehan PW, Coady TH, et al. The Wallerian degeneration slow (Wld(s)) gene does not attenuate disease in a mouse model of spinal muscular atrophy. Biochem Biophys Res Commun. 2008; 375:119–123. [PubMed: 18680723]
23. Ruiz R, Casanas JJ, Torres-Benito L, Cano R, Tabares L. Altered intracellular Ca^{2+} homeostasis in nerve terminals of severe spinal muscular atrophy mice. J Neurosci. 2010; 30:849–857. [PubMed: 20089893]
24. Seiler S, Kirchner J, Horn C, et al. Cargo binding and regulatory sites in the tail of fungal conventional kinesin. Nat Cell Biol. 2000; 2:333–338. [PubMed: 10854323]
25. Sumner CJ, Huynh TN, Markowitz JA, et al. Valproic acid increases SMN levels in spinal muscular atrophy patient cells. Ann Neurol. 2003; 54:647–654. [PubMed: 14595654]
26. Young SM Jr, Neher E. Synaptotagmin has an essential function in synaptic vesicle positioning for synchronous release in addition to its role as a calcium sensor. Neuron. 2009; 63:482–496. [PubMed: 19709630]
27. Zhang Z, Lotti F, Dittmar K, et al. SMN deficiency causes tissue-specific perturbations in the repertoire of snRNAs and widespread defects in splicing. Cell. 2008; 133:585–600. [PubMed: 18485868]
28. Zhao C, Takita J, Tanaka Y, et al. Charcot–Marie–Tooth disease type 2A caused by mutation in a microtubule motor KIF1Bbeta. Cell. 2001; 105:587–597. [PubMed: 11389829]
29. Zheng YL, Li BS, Veeranna Pant HC. Phosphorylation of the head domain of neurofilament protein (NF-M): a factor regulating topographic phosphorylation of NF-M tail domain KSP sites in neurons. J Biol Chem. 2003; 278:24026–24032. [PubMed: 12695506]

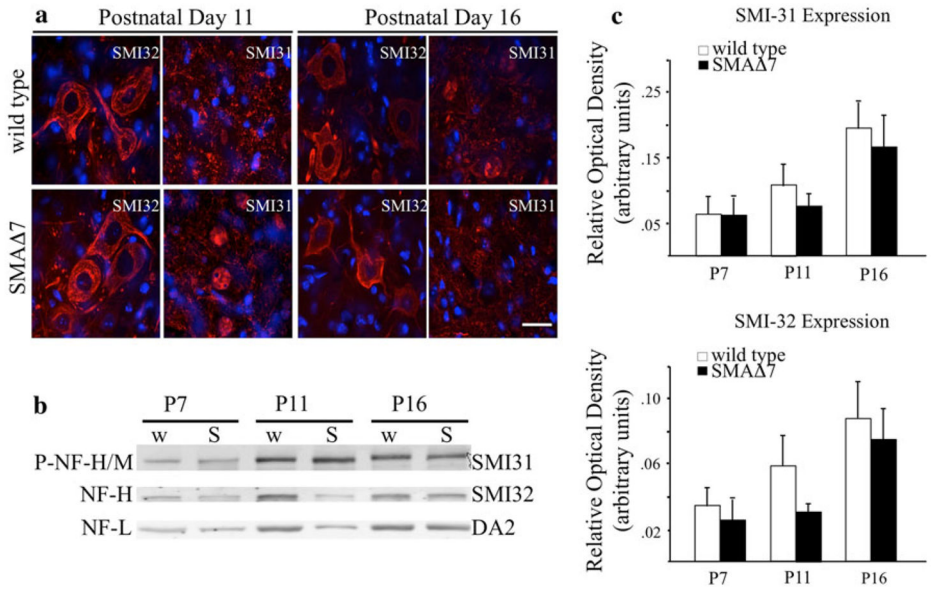

Fig. 1.

Ectopic accumulation of phosphorylated NFs does not occur in affected tissues of SMAΔ7 mice. Lumbar (**a**) spinal cord sections were immunostained with an antibody that recognizes dephosphorylated NFs (SMI-32) to identify motor neuron cell bodies. Ectopically phosphorylated NFs were identified with an antibody that recognizes NFs in a phosphorylated-dependent manner (SMI-31). NF localization was analyzed at both P11 and P16. Accumulation of ectopically phosphorylated NFs (*red*) was not observed in lumbar (**a**) motor neuron cell bodies, marked by nuclear DAPI staining (*blue*), at either time point. *Scale bar* 50 μm. NF phosphorylation and expression was not altered in SMAΔ7 (*S*) (*N* = 3) when compared with wild type (*w*) (*N* = 3) animals (**b**) shown by ROD analysis (**c**). Spinal cord lysates were separated on a 7.5% SDS polyacrylamide gels from wild type and SMAΔ7 mice at three different disease stages. Lysates were immunoblotted with antibodies recognizing phosphorylated NFs (SMI-31), unphosphorylated NFs (SMI-32) and a NF-L control (DA2). Statistical significance was determined by a Student's *t* test

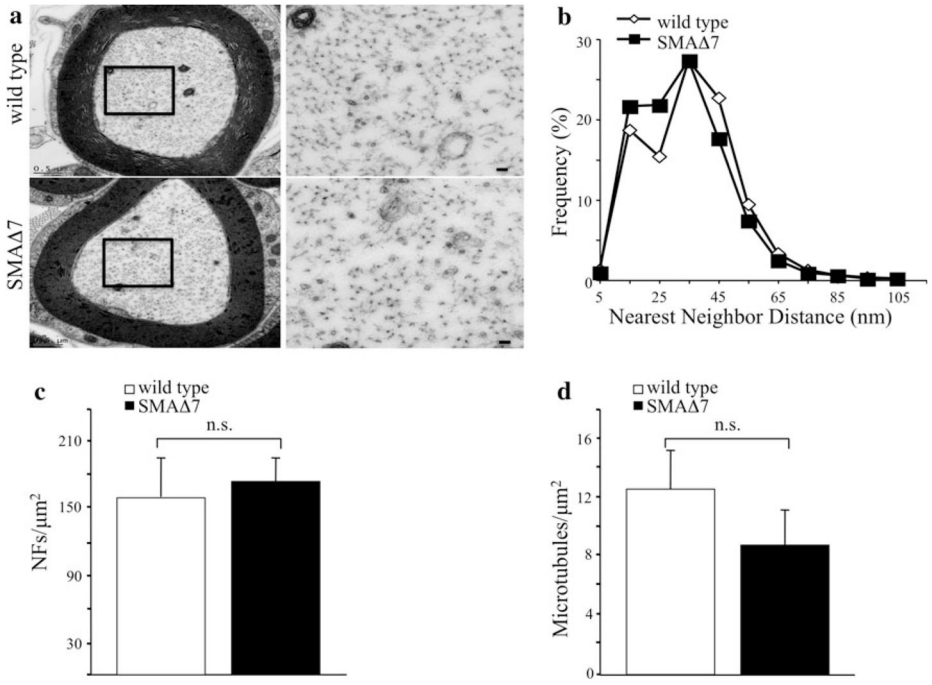

Fig. 2.

NF organization in proximal motor axons is unaffected in SMAΔ7 mice. Transmission electron micrographs of P12 motor axons derived from the fifth lumbar spinal root from wild type (*top N* = 9) and SMAΔ7 (*bottom N* = 7) mice used for nearest neighbor distances, NF densities, and microtubule densities (**a**). *Black box* identifies the region of the axon that is magnified to the *right* of each *micrograph. Scale bar* 500 nm. Distribution of nearest neighbor distances was slightly altered in SMAΔ7 mice. Each point represents the averaged distribution of axon diameters from the entire roots of at least seven mice for each genotype and age group. Distributions of nearest neighbor distances were analyzed for overall statistical differences using a Mann–Whitney *U* test. There was a statistically significant difference between nearest neighbor distances of SMAΔ7 versus wild-type mice ($P < 0.001$) (**b**). Densities of NFs (**c**) and microtubules (**d**) in SMAΔ7 and wild-type motor axons were unaltered. NF densities were analyzed for statistical significance by Student's *t* test, and microtubule densities were analyzed by Mann–Whitney test

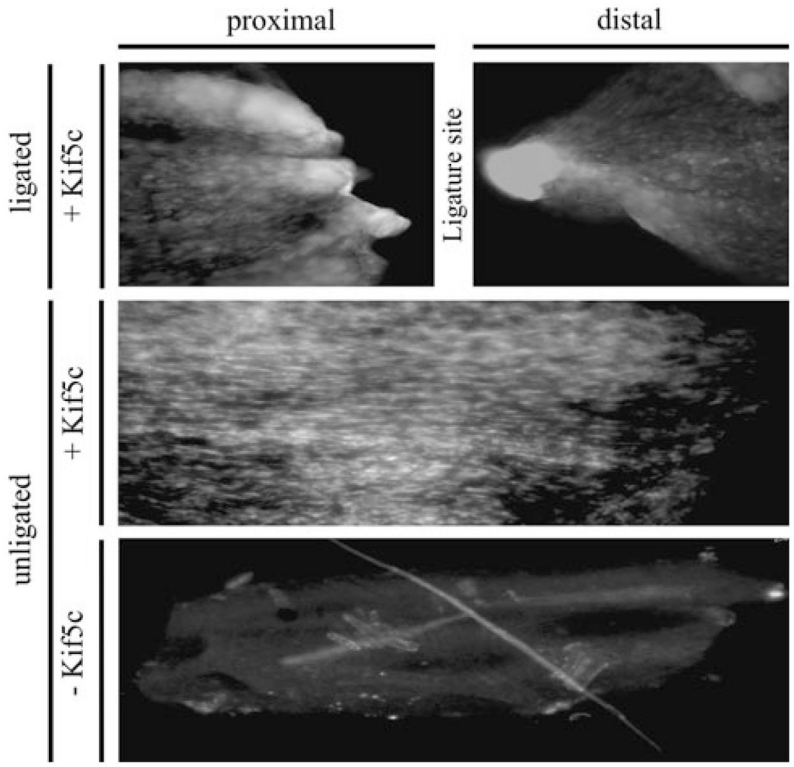

Fig. 3.

Kinesin accumulates proximal and distal to the ligation in P7 animals. Sciatic nerves were immunoblotted with (+Kif5C) and without (−Kif5C) an anti-kinesin antibody (Kif5c) in both ligated and unligated sciatic nerves. The proximal and distal nerve segments are identified, and the approximate location of the ligature site is indicated in ligated and unligated nerves

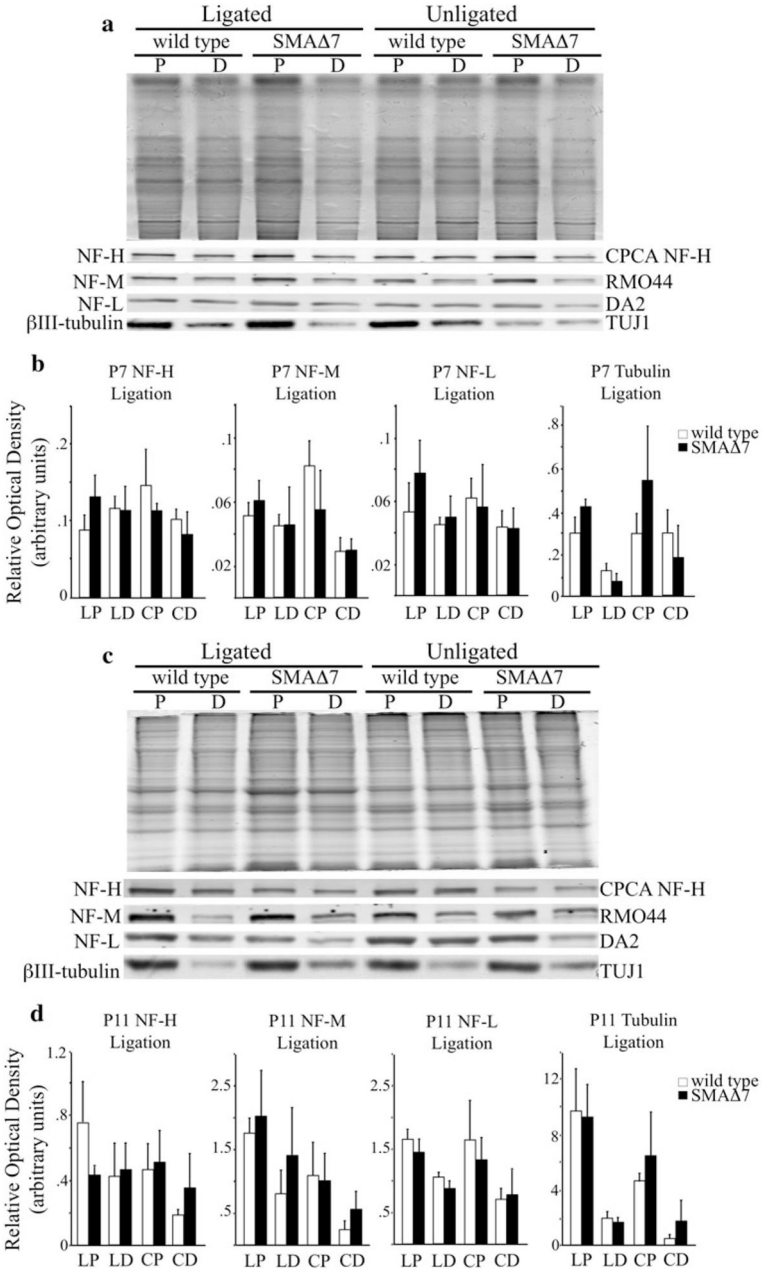

Fig. 4.

NF content is unaltered in the distal axon of SMAΔ7 mice. Sciatic nerves were ligated for 6 h, and equal length sections were dissected. Proximal (*P*) and distal (*D*) sciatic nerve lysates were separated on 7.5% SDS polyacrylamide gels from wild type (*N* = 3) and SMAΔ7 (*N* = 3) mice at two different disease stages. Lysates were immunoblotted with antibodies recognizing mouse NF-H (CPCA NF-H), NF-M (RMO44), NF-L (DA2) and a neuron-specific isoform of tubulin, βIII-tubulin (TUJ1). NF subunits and βIII-tubulin accumulated on the proximal side of the ligation in both SMAΔ7 and wild-type mice. There was no difference in the level of accumulation between SMAΔ7 and wild-type mice at P7 (**a**) or P11 (**c**) as determined by relative optical density (ROD) measurements (**b**, **d**). Statistical significance was determined by a Student's *t* test. *X* axis: proximal side of ligation (LP), distal side of ligation (LD), proximal section of unligated nerve (CP), distal section of

unligated nerve (CD). Simultaneously run coomassie stained gels were used as loading controls (**a**, **c** *top*)

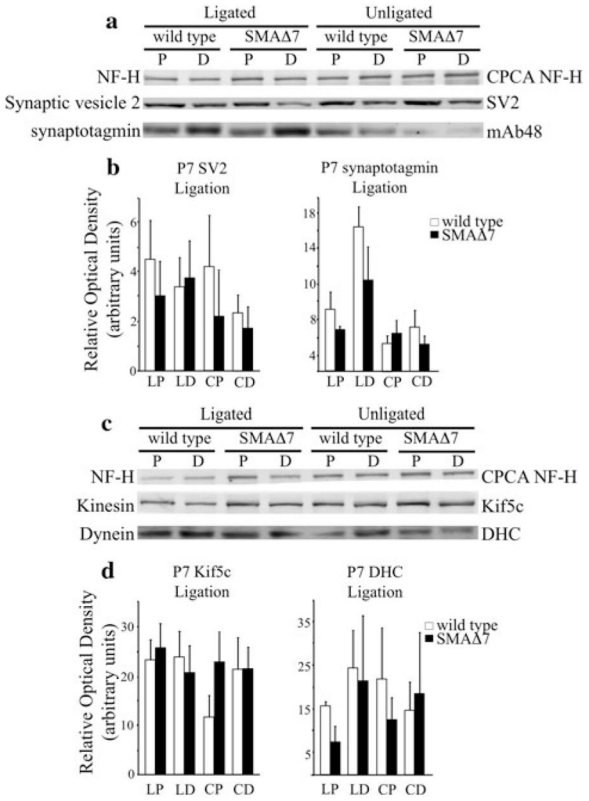

Fig. 5.

Fast, anterograde axonal transport is unaffected prior to the onset of observable phenotypes in SMAΔ7 mice. Sciatic nerves were ligated for 6 h in P7 wild type and SMAΔ7 littermates, and then harvested for analysis. Sciatic nerve lysates proximal and distal to the ligature were separated on 7.5% SDS polyacrylamide gels. Accumulation of synaptic vesicle proteins was analyzed (**a**). Based on ROD measurements (**b**), there was no difference in accumulation of SV2-c ($N = 3$) and Syt1 ($N = 5$) in SMAΔ7 mice. Accumulation of molecular motors that transport cargos in anterograde, Kif5c, and retrograde, dynein, directions was analyzed (**c**). There was no difference in the accumulation of Kif5c ($N = 4$) or dynein ($N = 3$) in P7 SMAΔ7 mice (**d**). Statistical significance was determined by a Student's *t* test. *X* axis: proximal side of ligation (LP), distal side of ligation (LD), proximal section of unligated nerve (CP), distal section of unligated nerve (CD). The heavy (**a**, **c** *top*) subunit of NFs was used as a loading control

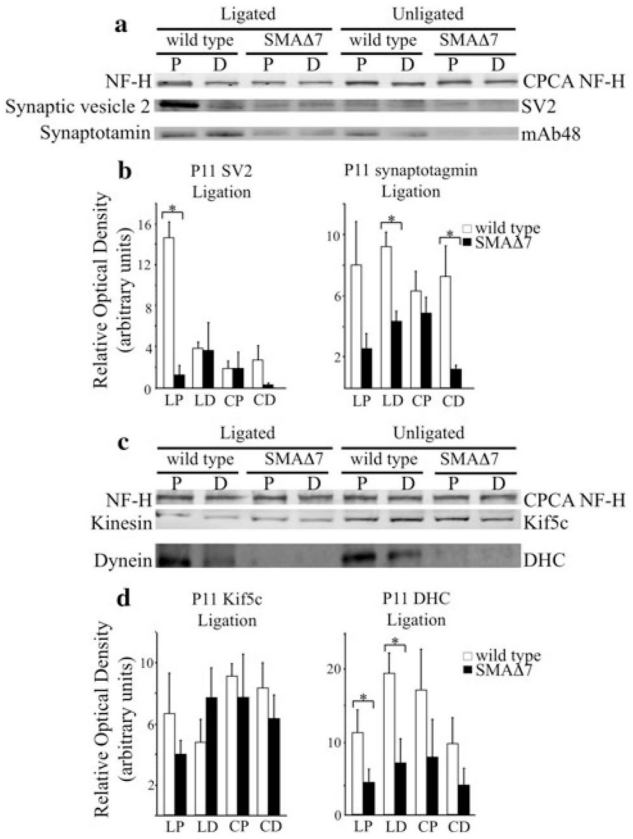

Fig. 6.

Fast, anterograde transport is reduced prior to observed reductions in synaptic vesicle densities. Sciatic nerves were ligated for 6 h in P11 wild type and SMAΔ7 littermates, and then harvested for analysis. Sciatic nerve lysates proximal and distal to the ligature were separated on 7.5% SDS polyacrylamide gels. Accumulation of synaptic vesicle proteins was analyzed (**a**). Accumulation of SV2-c ($N = 3$; $P < 0.001$) (**a**) was reduced in P11 SMAΔ7 mice as determined by ROD measurements (**b**). In addition, distal levels of Syt1 ($N = 4$; $P < 0.01$) in ligated and unligated nerves were reduced in P11 SMAΔ7 mice (**b**). Accumulation and steady state levels of Kif5c ($N = 3$) appeared unaffected in SMAΔ7 mice whereas both accumulation and steady state levels of dynein ($N = 4$; $P < 0.05$) were reduced (**c**, **d**). Statistical significance was determined by a Student's *t* test. *X* axis: proximal side of ligation (LP), distal side of ligation (LD), proximal section of unligated nerve (CP), distal section of unligated nerve (CD). The heavy (**a**, **c** *top*) subunit of NFs was used as a loading control

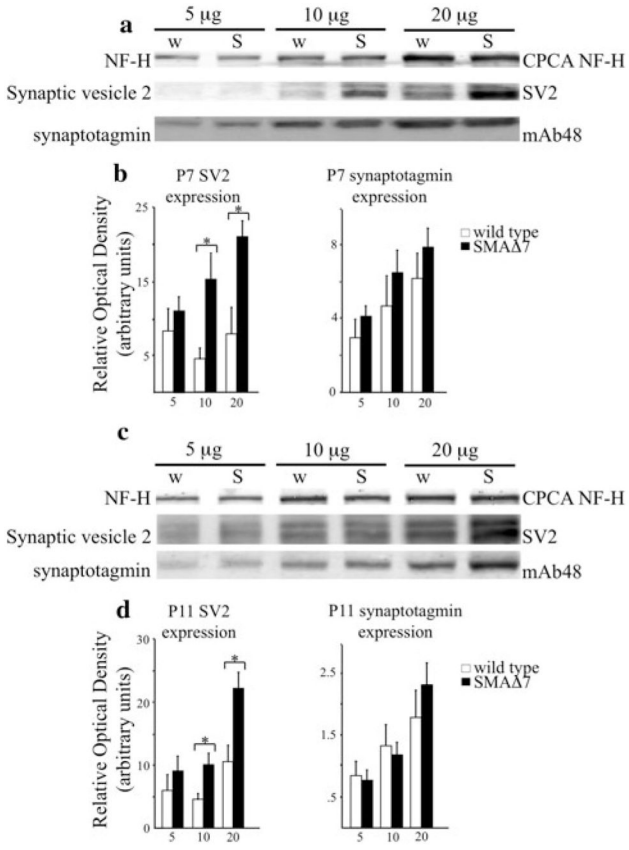

Fig. 7.

Reduction in transport of synaptic vesicle proteins is not due to reduced expression in SMAΔ7 mice. Three differing amounts of total protein (5, 10, and 20 µg) from spinal cord lysates were separated on 7.5% SDS polyacrylamide gels from wild type and SMAΔ7 mice at P7 (**a**) and P11 (**c**). Lysates were immunoblotted with antibodies recognizing SV2-c and Syt1 (mAb48). At P7 ($N = 3$; $P < 0.05$) and P11 ($N = 5$; $P < 0.05$), the spinal cord levels of SV2-c (**a**, **c** *middle*) were increased in SMAΔ7 mice. Relative expression levels were analyzed by ROD measurements (**b**). However, despite the reduction in transport and steady state levels observed at P11 for Syt1, spinal cord levels were unaffected in SMAΔ7 mice at P7 ($N = 3$) and P11 ($N = 5$) (**a**, **c** *lower*). Statistical significance was determined by a Student's *t* test. The heavy (**a**, **c** *top*) subunit of NFs was used as a loading control